Robustness evaluation of Bone Mineral Density measurements in spectral CT using Three Material Decomposition

Elixabete Ansorena

ABSTRACT

Background: Quantitative Computed Tomography (QCT) is, together with dual-energy X-ray absorptiometry (DXA), one of the most common methods for the measurement of Bone Mineral Density (BMD). The current approach for BMD evaluation relies on the manual placement of four Regions of Interest (ROI), one on the L1 vertebra, and further three in a reference phantom, which can be tedious, prone to human errors and is usually missing in routine CT scanning. New phantomless methods have been proposed for the measurement of BMD, namely the Three Material Decomposition Method (3MD), based on spectral imaging. In this study, we aim to study the regional variation of the BMD value across 13 different regions of the vertebra and evaluate the reproducibility of QCT-based BMD values using the 3MD method, where we also include the influence of cortical tissue, the venous plexus and the presence of lesions.

Methods: We selected 61 pseudoxanthoma elasticum (PXE) patients who received sprectral CT imaging. We calculated the BMD value using QCT and 3MD methods throughtout 11 different ROIs. In addition, we also evaluated the performance of two Volumes of Interest (VOI) placements, based on a deep-learning approach by Philips Healthcare. We also avoided the cortical tissue, venous plexus and lesions when positioning the ROI and VOIs to ensure accurate BMD readings. The corresponding BMD values were analysed to determine which area presented the closest results between QCT and 3MD.

Results: The VOI (Cleaned) placement presented the least difference between the QCT and 3MD techniques, displaying a mean difference of the 3MD method of 2.25% ± 24.80 . In contrast, the recorded largest mean difference amounted to 10.69% ± 33.76.

Conclusion: These findings indicate a VOI-based approach could be most beneficial for phantomless 3MD-based BMD measurements as long as the cortical tissue, venous plexus and lesions are taken into account. However, further development is necessary to address the large interpatient variation to support this argument confidently.

I. INTRODUCTION

Osteoporosis is a skeletal disease that changes the microstructure and properties of the bone. Affected regions display decreased levels in bone mass that increase the risk of fractures [1]. Due to the unpredictable nature of osteoporosis-related fractures, their occurrence can gravely impair a patient's life and even have lethal consequences [2]. Early diagnosis of osteoporosis is paramount to avoid the development of fractures and begin early treatment to deter further bone mass decline. In order to detect early signs of osteoporosis, the bone mineral density (BMD) must be estimated. The BMD is representative of the presence, and in what quantity, of minerals such as calcium hydroxyapatite (HA) within the bone and it is best observed on the trabecular tissue [3].

BMD can be measured by means of Quantitative Computed Tomography (QCT), one of the current clinical standards [4]. However, this method represents several disadvantages when performing BMD measurements [5]. QCT is prone to the underestimation of the BMD value proportionally to the presence of adipose tissue within the bone marrow. Furthermore, QCT also requires the use of an externally placed phantom to perform the estimation, which is often forgotten or badly placed.

Aiming to provide an alternative to QCT that would solve its fundamental issues, Three Material Decomposition (3MD) was proposed [6], based on Dual-Energy Computed Tomography (DECT) [7]. By acquiring a high- and a low energy spectra, DECT enables the generation of virtual mono-energetic (monoE) images, which display the Hounsfield Unit (HU) values as if the scans were acquired at a single photon energy. The combination of multiple monoE images (i.e. low- and high-energy) can enable the characterization of different tissue types based on their unique attenuation values at each energy. Being able to identify the presence of marrow fat allows of the 3MD algorithm to address the underestimation of the BMD value. Moreover, DECT allows for volumetric evaluation of the BMD without the need of a phantom, altogether addressing the phantom-related downfalls of QCT.

Both QCT and 3MD methods for measuring BMD rely on the manual placement of a circular Region of Interest (ROI) on the superior anterior region of the L1 vertebra. This approach entrusts the technician with performing an adequate placement of the ROI, avoiding cortical tissue, lesions and vessels alike. As a result, this process can be tedious and liable to innacuracies. To solve this, we developed an automatic ROI placement tool capable of evading cortical bone, lesions and other unsuitable tissue in order to aid in the unassisted evaluation of BMD.

In this study, we evaluated the robustness of the 3MD and QCT methods for the measurement of the BMD using an automatic ROI/VOI placement algorithm. Moreover, we analysed the regional susceptibility of BMD value based on location and ROI/VOI shape.

II. METHODS

A. Patient Selection

All 61 patients used in our study were provided by the UMC and acquired between January 2020 and January 2022. Subjects suffered from pseudoxanthoma elasticum (PXE), a genetic disorder that targets connective tissue, altering its mineral composition [9]. It should be noted that this disease does not affect the structural nor mineral integrity of vertebrae. The imaging requirements for the admittance in the study included a non-contrast-enhanced-CT scan carried out with a DLCT system (iQon Spectral CT, Philips Healthcare, Best, The Netherlands) and the availability of the respective spectral data. This resulted in a collection of 61 patients, whose characteristics can be found in Table 1.

Table 1: Sex and age (mean ± standard deviation) of included patients

	Number of patients	Age
All	61	59.32 ± 15.11
Female	28	60.06 ± 14.19
Male	33	58.65 ± 15.89

Moreover, a phantom (QRM GmbH, Moehrendorf, Germany) had to be present in the conventional CTs, placed at knee-height and with three different concentrations of HA, 0, 98.5 and 198.6 mg/cm^3 . The main body of the phantom was produced using water-equivalent polymers, with an attenuation value comparable to that of water. The HA in the phantoms will be necessary to estimate the calcium concentration within the trabecular bone by means of linear regression and compute the BMD for the QCT method.

B. Image Acquisition

The conventional CTs were acquired using a spiral acquisition mode with a tube peak voltage of 120 kV and 0.984 pitch factor, where the gantry revolution time was 0.75s and using a 64x0.625 collimation system. Radiation exposure was controlled by means of adapting the tube current to the size of the patient all the while maintaining the signal-to-noise ratio.

Both conventional and monoE images of 50 and 200 keV were reconstructed based on the Spectral Base Image (SBI) with a standard filter kernel (B) and slice thickness of 1 mm [10].

Finally, the segmentation of the L1 vertebra was obtained by means of a whole spine segmentation algorithm provided by Philips Healthcare. This tool, based on deep learning, identified the L1 vertebra within the spine and provided its labelmap in NIFTI format.

C. Automatic ROI placement algorithm

We developed an automatic ROI placement algorithm to aid in the evaluation of the optimum positioning of the ROI within the vertebra. In order to perform an unassisted placement of the ROI, the automatic placement algorithm needed to avoid three types of tissue: cortical bone, venous plexus and lesions. The ultimate goal of the tool will be to place the ROI in as much clean trabecular bone as possible, given the bone microstructure is not homogeneous, and a large area of analysis provides more robust BMD results.

In total, eleven ROIs were placed, located in the anterior, middle, posterior, left and right regions of the vertebra. These ROIs were distributed in three levels of the vertebral body, superior (5 ROIs), middle (1 ROI) and inferior (5 ROI).

The first step when designing this tool was the removal of the cortical tissue, which is characterized as the bright intensities surrounding the vertebra. This process was conducted by means of morphological erosion, as depicted in Figure 1.

The morphological erosion operates under the basis that the cortical tissue is uniform along its thickness around the entire vertebra, which is not necessarily true. Aiming

to ensure all cortical tissue was removed, we evaluated the outer perimeter of the eroded segmentation to ensure no remaining cortical pixels were still included in the segmentation.

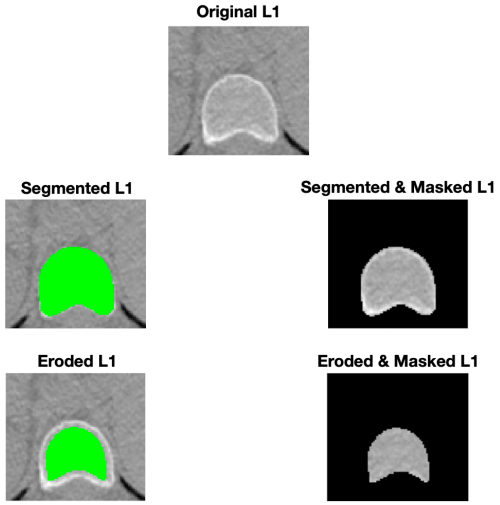

Figure 1: Morphological erosion operation using a disk 4 structuring element for cortical tissue removal.

We first obtained a reference value of the trabecular tissue by computing the mode of the eroded vertebra, given it is primarily trabecular tissue. Based on that value, we considered cortical tissue to be those intensities that exceeded the threshold by a margin of 20% [11].

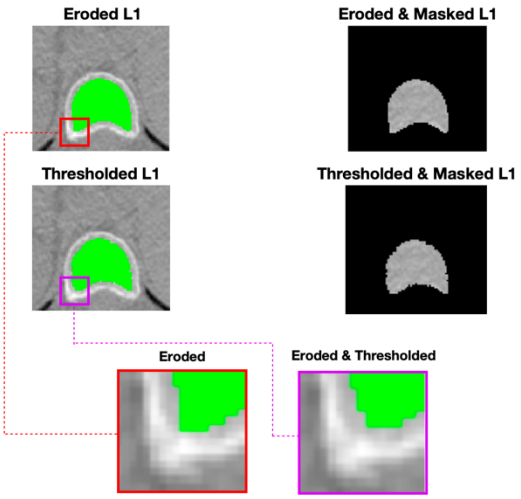

Figure 2: Thesholding method based on the mode of vertebra to clean up any remaining cortical tissue.

As displayed in Figure 2, if the erosion fails to remove all cortical tissue, the remaining cortical pixels will be eliminated by the thresholding, which will be solely applied to the two-pixel thick outer perimeter of the vertebra.

Once all the cortical tissue was removed, the next step consisted of identifying the location of the venous plexus. The venous plexus is the group of veins that irrigate the vertebra and have their entry point in the middle level of the vertebral body [12]. This structure is not always visible in CT scans, which is the reason why we consulted with clinicians and opted to assume that the venous plexus will be located exactly in the middle plane of the vertebra and traverse until its center.

The venous plexus enters the vertebra in a perpendicular angle relative to its inclination, which meant we first had to determine the tilt of the L1. We completed this by automatically identifying the two peaks in each end of the posterior face of the vertebra. In order to do so, we first computed the one-pixel thick outline of the vertebra. We then selected those pixels that corresponded to the posterior face of the L1. To avoid any other lose pixels to be detected, we considered the target structure to be the one with the biggest connected area. Finally, we assumed the first and last pixels of these countour to be corresponding to the peaks of the vertebra. After that, we proceeded to calculate their angle as opposed to a vertical plane. Next, we computed the centroid of the sagittal plane of the vertebra, which would define the depth of the venous plexus. Knowing that the average venous plexus occupies about a fifth of the vertebral height [13], we defined the final height of the vascular structure. This process is further illustrated in Figure 3.

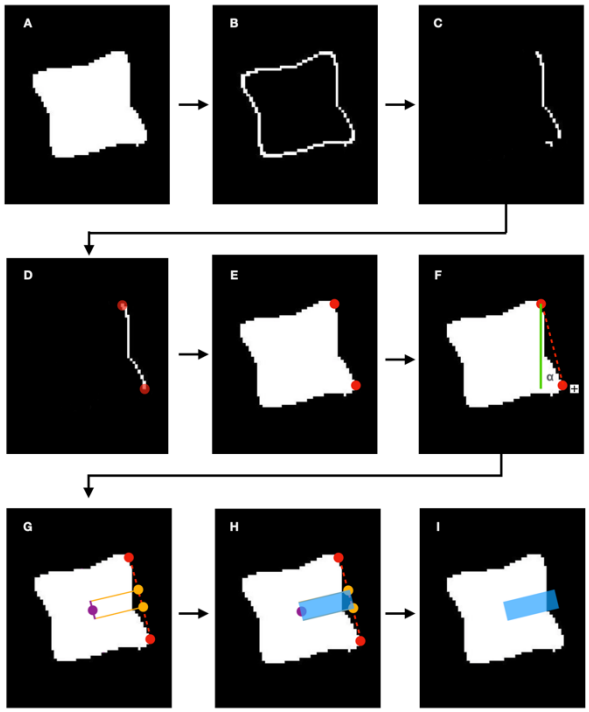

*Figure 3: **A**; Original L1 Segmentation. **B**; One-pixel thick outer perimeter. **C**; Isolated posterior face of vertebra. **D**; Cleaned posterior face with red highlights in first and last pixels. **E**; Two peaks of the posterior face. **F**; Inclination of vertebra, given by angle alfa. **G**; Centroid (in purple), defining depth of venous plexus and width (in orange), defining the height of venous plexus. **H**; Estimated location of venous plexus. **I**: Isolated venous plexus.*

After locating the venous plexus, we define the levels wherein the ROIs would be located. The middle level will be in the center of the vertebra, passing through the centroid (purple point, Figure 3) we used to define the depth of the venous plexus.

Regarding the superior level, we defined this using two points as reference. The top limit of the superior level is determined by the height of the superior anterior edge of the L1, that is, the first full-width slice of the vertebral cross-section. On the other hand, the bottom limit of the superior level is chosen based on the height of the highest point of the venous plexus to ensure no region of its structure will be placed inside the ROI. Finally, based on that margin, the middle slice will be the one used to complete the ROI positioning. This same logic was used to define the inferior level. The procedure is illustrated by Figure 4.

Next, the ROI placement was performed. The ROIs used for this purpose measured 14 pixels in diameter and had a width of three slices [14].

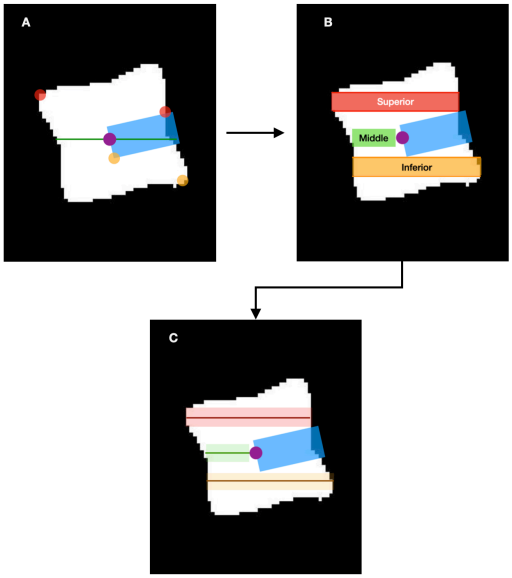

*Figure 4: Slice level selection prodecure. **A:** Reference points based on venous plexus height and vertebral slice width. **B:** Displayed margins for posible level selection. **C:** In bold, the middle slices of the marging presented in subfigure **B**, corresponding to the final slice levels.*

We began with the superior level, where five ROIs were placed. It should be noted that the positioning decisions behind all ROIs have been made based on medical advice. First, we positioned the middle ROI, its location being determined by the centroid of the slice. Then, we moved on to the posterior ROI, placed seven pixels above the middle one, corresponding to the radius of the ROI . We repeated the operation for the anterior ROI, this time making it seven pixels lower than the middle ROI. Finally, we placed the left and right ROIs seven pixels to the sides of the anterior ROI. This is further illustrated by Figure 5.

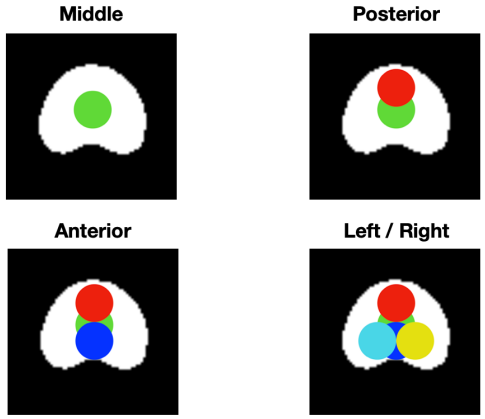

Figure 5: Process of ROI positioning. Green: Middle. Red: Posterior. Blue: Anterior. Cyan: Left. Yellow: Right.

We repeated the same process to place another five ROIs in the inferior level and a single posterior ROI in the middle level. It should be noted that the 3-slice thickness of the ROIs is achieved by extending the previously placed ROI one slice up and one slice down.

Finally, we accounted for the possible lesions present within the trabecular bone. However, instead of looking for all lesions present in the vertebra, only those areas within the ROI were analysed. The interior of each ROI was evaluated for the presence of hyper or hypointense pixels, far from the common intensities of trabecular bone, once again defined by the mode of the L1. If more than 20% of the interior of the ROI presented non-trabecular intensity values, the ROI was rejected.

After accounting for the cortical tissue, venous plexus and lesions, the algorithm provided 11 different NIFTI files corresponding to each individual ROI positioning.

D. Alternative VOI placement by Philips Healthcare

Although current clinical consensus establishes the BMD must be measured using a circular ROI, Philips Healthcare manifested their interested in evaluating the possibility of performing a BMD measurement using a Volume of Interest (VOI). Given that CT allows for 3D imaging, we hypothesize that spherical VOI might provide more robust solutions compared to 2D ROIs. This VOI, determined automatically by their deep-learning-based spine segmentation algorithm, is located in the centroid of the vertebra, as depicted in Figure 6.

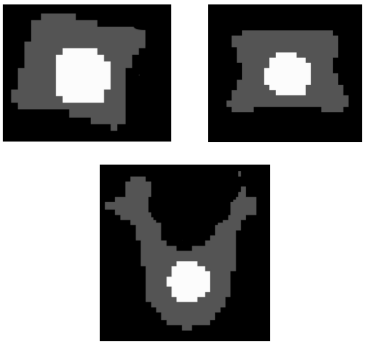

Figure 6: VOI positioning and shape example in 3 different slices provided by Philips Healthcare.

It should be noted that this VOI placement does not account for the presence of cortical tissue, lesions or venous plexus within its bounds. In response to that, and aiming to evaluate the effect this might have in the BMD measurements, we also analysed a version of this VOI where these three tissues were removed using the same algorithm employed with the ROIs. Examples of both VOIs are displayed in Figure 7.

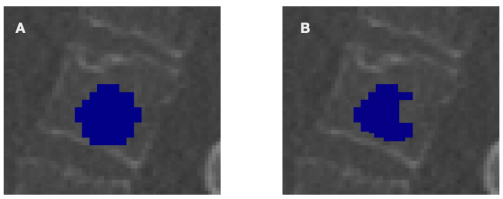

*Figure 7: **A:** Original PHVOI. **B:** Cleaned PHVOI.*

E. QCT and 3MD-based BMD measurement

The first the step after obtaining the ROIs and the VOI from Philips Healthcare (PHVOI), was to measure each of their BMD value using the QCT method. This was performed using an in-house developed [14] algorithm that computed the final BMD by linearly correlating the values of the phantom to the values inside the ROIs. In order to consider the values of the phantom, we placed ROIs corresponding to the 0, 98.5 and 198.6 mg/cm^3 values of HA, depicted in Figure 8.

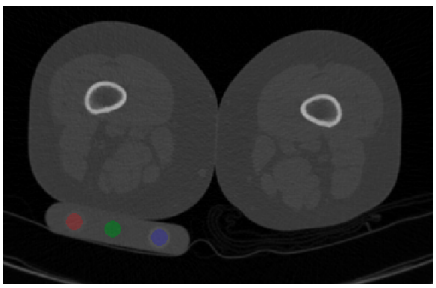

Figure 8: BDC phantom placement instance in a conventional CT. In red, green and blue, the corresponding ROI labels to the HA concentrations of 98.5, 0 and 198.6 mg/cm^3, respectively.

Next, we performed the same analysis but this time using the 3MD method for BMD measurement. The code used for this purpose was once again in-house developed [14] and it uses a non-linear least square approach to determine the volume fractions of HA, water and marrow adipose tissue in a given region [6].

After having processed all patients for both 3MD and QCT-based BMD measurement for all 11 ROIs and the two PHVOIs, we performed the statistical analysis. Figure 9 exemplifies one instance of these BMD measurements.

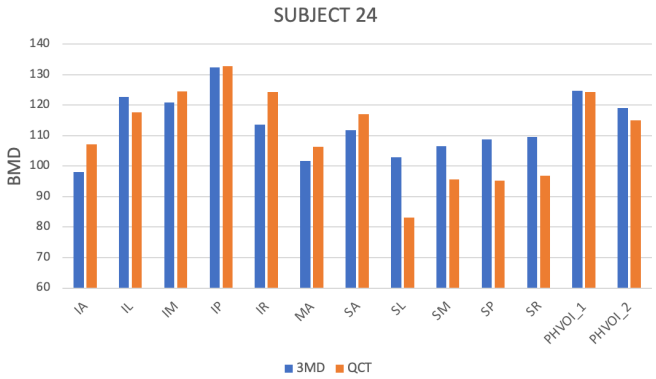

Figure 9: 3MD and QCT-based BMD measurement comparison for Subject 24 throughout 11 ROIs and PHVOIs. PHVOI_1 corresponds to the original PHVOI and PHVOI_2 to the cleaned.

F. Statistical Analysis

The aim of the statistical analysis was to compare the differences in BMD value between the QCT and 3MD methods thorughout the 11 different ROI and PHVOI placements, as to determine which ROI/PHVOI offered the most consistent and accurate results.

First, we computed the percentage difference between QCT and 3MD-based BMD measurements for each ROI and PHVOI placement throughout all 61 patients. An example of this operation is illustrated in Figure 10, corresponding to the IA ROI.

The values displayed in Figure 10 portray the performance of each ROI/PHVOI for the BMD measurement and how much the 3MD method under or overestimated its value with QCT as reference.

Next, we obtained the mean change in BMD per ROI and PHVOI, which allowed us to rank each location as a function of its accuracy when measuring the BMD. Using the IA ROI as an example once again, its mean percentage difference was that of 3.18 %.

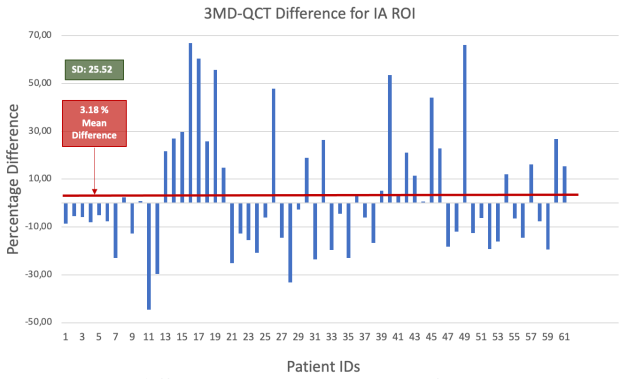

Figure 10: Mean difference percentage in BMD for IA ROI positining.

We repeated this process for all 61 patients accross all 11 ROIs and the PHVOIs, recording their mean differences and SD in BMD values.

III. Results

We gathered all 13 mean differences for BMD and SD and ranked the ROIs and PHVOIs based on it, as Table 1 showcases.

Table 2: Ranked BMD and SD percentage difference between 3MD and QCT for 11 ROIs and PHVOIs.

Position	BMD % ± SD	SD (ROI) % ± SD
PHVOI (Cleaned)	2.25 ± 24.80	-24.78 ± 22.14
PHVOI (Orig)	2.28 ± 17.48	-27.89 ± 27.12
IA	3.18 ± 25.52	-28.37 ± 22.88
SA	3.36 ± 29.14	-23.51 ± 46.88
IR	4.37 ± 21.04	-20.48 ± 33.50
SM	5.04 ± 28.09	-23.46 ± 36.71
IP	5.13 ± 23.57	-27.41 ± 22.71
MA	5.97 ± 24.97	-24.09 ± 42.91
IM	6.46 ± 25.59	-25.97 ± 33.44
SP	6.51 ± 29.56	-20.28 ± 41.18
IL	6.70 ± 25.10	-18.60 ± 39.09
SR	7.09 ± 25.82	-19.78 ± 28.43
SL	10.69 ± 33.76	-23.20 ± 44.83

The cleaned PHVOI displayed the closest results in BMD value between 3MD and QCT, recording an average difference of 2.25% ± 24.80 and closely followed by the original PHVOI at 2.28% ± 17.48. In contrast, we concluded that SL displays the biggest variation between BMD measurement techniques, with 10.69% ± 33.76.

Aiming to evaluate the effect of removing the cortical tissue, venous plexus and lesions, we compared the BMD values obtained with the PHVOIs to the mean BMD value from the 11 ROIs for each of the 61 patients. The results are displayed in Figure 11 and Figure 12.

As Figure 11 indicates, the original PHVOI records 3MD-based BMD values that are consistently higher than those obtained throughout the 11 ROIs. This is illustrated in subfigure A by those patients that fall under the reference line, indicating their PHVOI-based BMD is higher than the ROI-based counterpart. In the case of the 3MD method, this occurs in 45 out of 61 patients, and the mean BMD increase equals 10.30%. On the other hand, when accounting for the cortical tissue, venous plexus and lesions, and repeating this analysis, we obtained subfigure B, where a closer relationship can be observed between both types of measurements. In this case, only 26 out of 61 patients recorded higher BMD values, but more importantly, the mean BMD difference decreased to 6.98%.

Regarding the QCT-based BMD values, we observed the same phenomenon in Figure 12. Subfigure C showcases the large differences in BMD between the mean ROIs and original PHVOI, 41 out of 61 patients falling below the reference line. Moreover, for this specific method, the mean BMD increase registered for the original PHVOI was that of 12.2%. After applying the cleaning algorithm to remove unwanted tissue, and showcased in subfigure D, the data indicated that 47 out of 61 patients displayed larger BMD values for PHVOI compared to the mean ROIs. Although the number of patients increased slightly, the mean difference was largely reduced, down to 4.42%.

IV. Discussion

The performance of 11 ROI and two PHVOI positionings was evaluated to determine the optimum region of the vertebra for 3MD-based BMD measurement.

In line with the research conducted by Offenberg [14], we found that the 3MD method tends to overestimate the value of the BMD in relation to the QCT method in all regions of the L1. This phenomenon can be observed in the second column of Table 1, where all the positive percentage values indicate that the BMD values recorded were generally higher with the 3MD method. Furthermore, we also found out that the 3MD approach largely affects the SD of the tests. Once again referencing Table 1, the all-negative values of the third column indicate the reduction on the SD for the 3MD-based BMD values. However, all these results possess elevated SD values, which suppose a liability when reaching a definite conclusion.

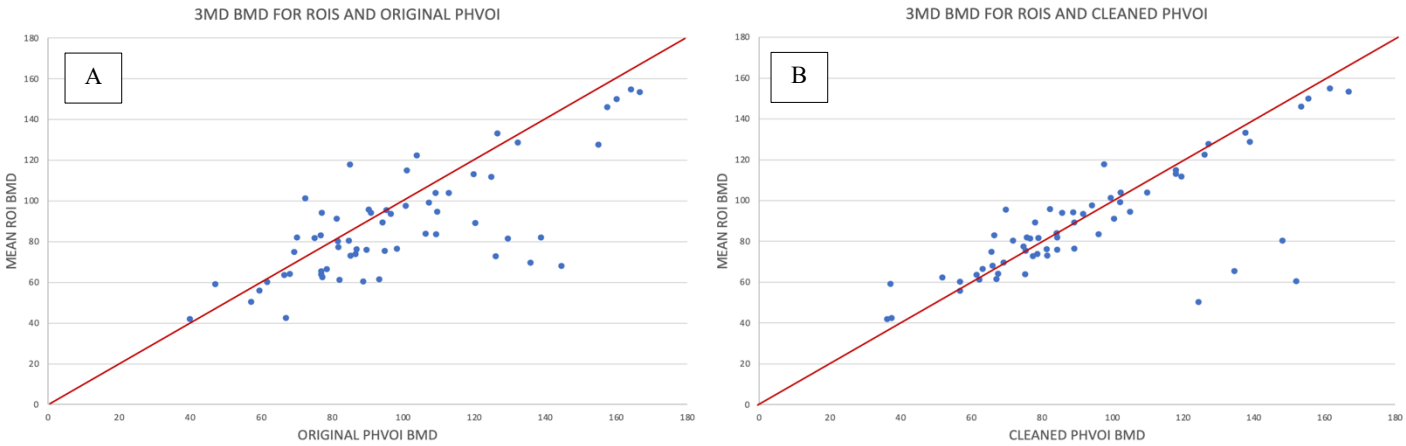

Figure 11: Plots showcasing the relationship in BMD values using the 3MD method for the PHVOIs and the mean of all ROIs

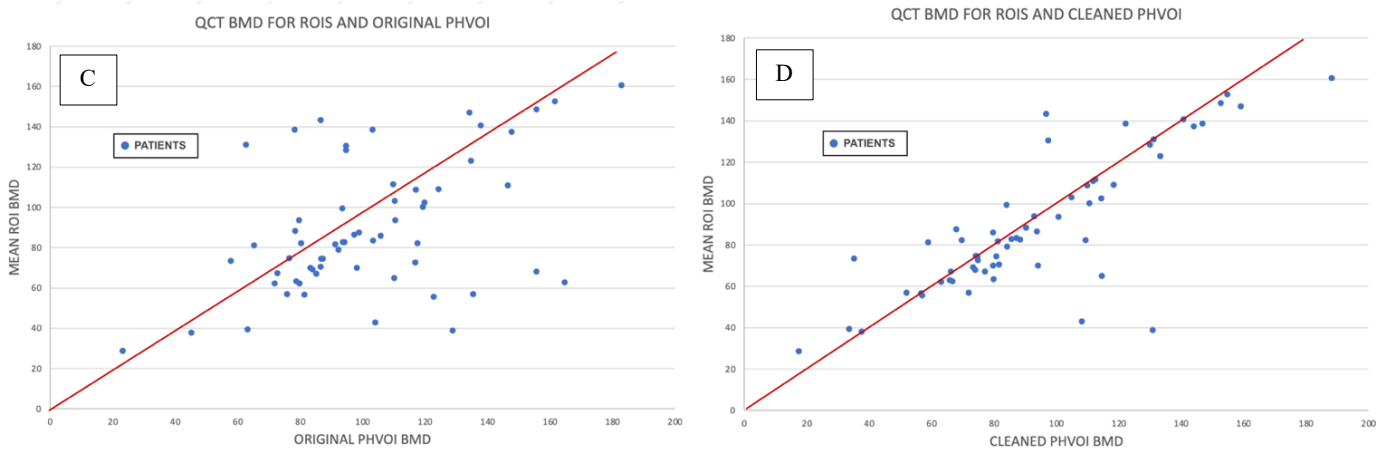

Figure 12: Plots showcasing the relationship in BMD values using the QCT method for the PHVOIs and the mean of all ROIs.

Even though we discovered that the cleaned PHVOI obtained the closest results between 3MD and QCT, we should take into account that there is only a 8% difference between the best (PHVOI, Cleaned) and worst (SL) ranking regions of the vertebra. Moreover, we must also consider the SD values we disclosed in Table 1. All the ROI and PHVOIs posses SD values that fall within the margin of the BMD measurements, meaning that the percentage differences we recorded are once again liable to large deviation that could reorganize the ranking. As a result, we should aim to reduce the SD values of both methods to confidently state that the cleaned PHVOI is the best positioning technique for 3MD-based BMD measurement. An option to reduce the SDs would be to add another set of spectral images, captured at 70 KeV for example, to further increase the certainty of the measurements.

When it comes to improving the overall positioning of the ROIs and PHVOIs, we believe the biggest margin lies on the detection of the venous plexus. There is currently not enough research that confidently denotes the location of this vascular structure, leading us to rely on the advice of physicians for a big part of the design of our algorithm.

Moreover, we also consider the cortical tissue and lesion removal section of the algorithm to have potential for improvement. Although the basic morphological erosion followed by the thresholding performed adequately for our purpose, we are confident opting for a more advanced erosion technique, such as, adaptative erosion, would provide a more accurate removal of the cortical tissue. Regarding the lesion removal, we consider further research is necessary to support our approach based on the 20% rule. However, we do not consider this had major effect in our thesis, given our cohort of patients did not present many vertebral lesions.

Applying these improvements to both the ROI and PHVOI placement algorithms, while improving the SD of the measurement techniques would amount to a more accurate reading of the BMD values.

V. CONCLUSION

In this thesis, we evaluated the performance of 13 different regions for the measurement of 3MD-based BMD value. The results indicate the cleaned PHVOI obtains the most accurate results when compared to the current clinical standard QCT. However, the SD values that were recorded indicate that further development is necessary to improve the precision of the tests and confidently state the PHVOI-based approach is the optimum one. Moreover, it would be advised that future versions of the deep-learning algorithm by Philips Healthcare consider the presence of cortical tissue, venous plexus and lesions, avoidable characteristics that would amount for a more accurate reading of the BMD value. In conclusion, this thesis showed promising results to pursue the use of VOI-based BMD measurements.

VI. ABBREVIATIONS

SA	Superior Anterior
SP	Superior Posterior
SM	Superior Middle
SR	Superior Right
SL	Superior Left
IA	Inferior Anterior
IP	Inferior Posterior
IM	Inferior Middle
IR	Inferior Right
IL	Inferior Left
MA	Middle Anterior

VII. ACKNOWLEDGEMENT

I thank my supervisor dr. ir. Koen Vincken and dr. Graeme Campbell for their guidance and assistance during the completion of this project. Moreover, I am also most grateful for the clinical advice received from dr. Wouter Foppen, prof. dr. Pim de Jong and dr. Arnold Schilham.

VIII. REFERENCES

[1] Pisani, P., Renna, M. D., Conversano, F., Casciaro, E., Di Paola, M., Quarta, E., Muratore, M., & Casciaro, S. (2016). Major osteoporotic fragility fractures: Risk factor updates and societal impact. *World journal of orthopedics*, *7*(3), 171–181. https://doi.org/10.5312/wjo.v7.i3.171

[2] Office of the Surgeon General (US). Bone Health and Osteoporosis: A Report of the Surgeon General. Rockville (MD): Office of the Surgeon General (US); 2004. 5, The Burden of Bone Disease.

[3] Marshall, D., Johnell, O., Wedel, H. Meta-analysis of how well measures of bone mineral density predict occurrence of osteoporotic fractures BMJ 1996; 312 :1254 doi:10.1136/bmj.312.7041.1254

[4] Thomas, M., Link, Thomas, F. Lang, Axial QCT: Clinical Applications and New Developments, Journal of Clinical Densitometry, Volume 17, Issue 4,2014,Pages 438-448, ISSN10946950, https://doi.org/10.1016/j.jocd.2014.04.119

[5] Link, T.M., and Kazakia, G., "Update on Imaging-Based Measurement of Bone Mineral Density and Quality," Current Rheumatology Reports, vol. 22, no. 5. Springer, May 01, 2020, doi: 10.1007/s11926- 020-00892-w.

[6] Hofmann, P. et al., "Phantom-less bone mineral density (BMD) measurement using dual energy computed tomography-based 3- material decomposition," Med. Imaging 2016 Comput. Diagnosis, vol. 9785, p. 97853E, 2016, doi: 10.1117/12.2217413.

[7] van Hamersvelt, R. W. et al., "Accuracy of bone mineral density quantification using dual-layer spectral detector CT: a phantom study," Eur. Radiol., vol. 27, no. 10, pp. 4351–4359, Oct. 2017, doi: 10.1007/s00330-017-4801-4.

[8] Van Ommen, F., H. W. A. M. De Jong, J. W. Dankbaar, E. Bennink, [22] T. Leiner, and A. M. R. Schilham, "Dose of CT protocols acquired in clinical routine using a dual-layer detector CT scanner: A preliminary report," 2019, doi: 10.1016/j.ejrad.2019.01.011.

[9] Germain, D. P., "Pseudoxanthoma elasticum," Orphanet J. Rare Dis. 2017 121, vol. 12, no. 1, pp. 1–13, May 2017, doi: 10.1186/S13023- 017-0639-8.

[10] Roski, F. et al., "Bone mineral density measurements derived from dual-layer spectral CT enable opportunistic screening for osteoporosis," Eur. Radiol., vol. 29, no. 11, pp. 6355–6363, Nov. 2019, doi: 10.1007/s00330-019-06263-z.

[11] Zhang, R. J., Li, H. M., Gao, H., Jia, C. Y., Xing, T., & Shen, C. L. (2020). Associations between the hounsfield unit values of different trajectories and bone mineral density of vertebrae: cortical bone and traditional trajectories. *American journal of translational research*, *12*(7), 3906–3916.

[12]Carpenter, K., Decater, T., Iwanaga, J., Christopher M. Maulucci, C.J. Bui, Aaron S. Dumont, R. Shane Tubbs, Revisiting the Vertebral Venous Plexus–A Comprehensive Review of the Literature,World Neurosurgery,Volume 145,2021 Pages 381-395,ISSN 1878-8750.

[13] Groen, R.J., Groenewegen, H.J., van Alphen, H.A., Hoogland, P.V., Morphology of the human internal vertebral venous plexus: a cadaver study after intravenous Araldite CY 221 injection. Anat Rec. 1997.

[14] Offenberg, R. Phantomless bone mineral density assessment in patients using dual-energy CT. Utrecht University, UMC, Minor Research Project 2021.

Layman Summary

Osteoporosis is a disease that can have lethal consequences, which is why its early detection is crucial. New methods for osteoporosis diagnosis based on bone mineral density (BMD) measurement have been proposed, namely Three Material Decomposition (3MD). In this new study, we evaluate the performance of the 3MD against one of the current clinical standards, Quantitative Computed Tomography (QCT). We studied the regional variability of the 3MD method and determined the optimum region of the L1 vertebra for the automatic placement of a region of interest (ROI). With this goal, we developed an automatic ROI placement algorithm capable of avoiding unwanted tissues, such as, cortical bone, venous plexus and lesions. We evaluated 11 different positionings of circular ROIs, together with two spherical volumes of interest (VOI) placed around different levels of the vertebral height and proposed by Philips Healthcare. The result of this analysis indicated that the placement of a cleaned VOI provides the closest BMD values between 3MD and QCT methods, with a mean difference of 2.25%. However, we recorded large standard deviation values, meaning the precision of the tests must be improved to definitely identify an optimum region for VOI placement within the L1 vertebra. Overall, we believe accounting for the cortical tissue, venous plexus and lesions is critical in order to obtain accurate readings of the BMD value.